

# Expression and properties of hyperpolarization-activated current in rat dorsal root ganglion neurons with known sensory function

L. L. Gao<sup>1,2</sup>, S. McMullan<sup>3</sup>, L. Djouhri<sup>4</sup>, C. Acosta<sup>1</sup>, A. A. Harper<sup>5</sup> and S. N. Lawson<sup>1</sup>

<sup>1</sup>School of Physiology and Pharmacology, Medical Sciences Building, University of Bristol, Bristol BS8 1TD, UK

<sup>2</sup>Department of Physiology, Tongji Medical School, Huazhong University of Science and Technology, Wuhan, 430030, China

<sup>3</sup>Australian School of Advanced Medicine, Macquarie University, Sydney 2109, Australia

<sup>4</sup>Department of Molecular and Clinical Pharmacology, University of Liverpool, Liverpool, UK

<sup>5</sup>College of Life Sciences, University of Dundee, Dundee DD1 5EH, Scotland, UK

## Key point

- $I_h$  is a hyperpolarisation-activated current that influences neuronal excitability and is present in some sensory neurons.
- The magnitude and properties of  $I_h$  in different groups of sensory neurons that respond to painful stimuli (nociceptors) or to non-painful stimuli, such as low threshold mechanoreceptors (LTMs), were unknown.
- We found that neurons with the greatest  $I_h$  were the nociceptors and LTMs with the fastest conducting fibres. The highest  $I_h$  of all was present in LTM neurons that sense muscle stretch and length (muscle spindle afferents).
- The high levels of  $I_h$  could fundamentally influence excitability of fast conducting sensory neurons which detect muscle stretch/length, touch and pressure, and painful stimuli.  $I_h$  could thus influence sensations associated with all these.
- The properties of  $I_h$  are similar to those of HCN1- and HCN2-related  $I_h$ , suggesting that these channels underlie the current.

**Abstract** The hyperpolarization-activated current ( $I_h$ ) has been implicated in nociception/pain, but its expression levels in nociceptors remained unknown. We recorded  $I_h$  magnitude and properties by voltage clamp from dorsal root ganglion (DRG) neurons *in vivo*, after classifying them as nociceptive or low-threshold-mechanoreceptors (LTMs) and as having C-, A $\delta$ - or A $\alpha/\beta$ -conduction velocities (CVs). For both nociceptors and LTMs,  $I_h$  amplitude and  $I_h$  density (at  $-100$  mV) were significantly positively correlated with CV. Median  $I_h$  magnitudes and  $I_h$  density in neuronal subgroups were respectively: muscle spindle afferents (MSAs):  $-4.6$  nA,  $-33$  pA pF $^{-1}$ ; cutaneous A $\alpha/\beta$  LTMs:  $-2.2$  nA,  $-20$  pA pF $^{-1}$ ; A $\beta$ -nociceptors:  $-2.6$  nA,  $-21$  pA pF $^{-1}$ ; both A $\delta$ -LTMs and nociceptors:  $-1.3$  nA,  $\sim -14$  pA pF $^{-1}$ ; C-LTMs:  $-0.4$  nA,  $-7.6$  pA pF $^{-1}$ ; and C-nociceptors:  $-0.26$  nA,  $-5$  pA pF $^{-1}$ .  $I_h$  activation slow time constants (slow  $\tau$  values) were strongly correlated with fast  $\tau$  values; both were shortest in MSAs. Most neurons had  $\tau$  values consistent with HCN1-related  $I_h$ ; others had  $\tau$  values closer to HCN1+HCN2 channels, or HCN2 in the presence of cAMP. In contrast, median half-activation voltages ( $V_{0.5}$ ) of  $-80$  to  $-86$  mV for neuronal subgroups suggest contributions of HCN2 to  $I_h$ .  $\tau$  values were unrelated to CV but were inversely correlated with  $I_h$  and  $I_h$  density for all non-MSA LTMs, and for A $\delta$ -nociceptors. From activation curves  $\sim 2$ – $7\%$  of  $I_h$  would be activated at normal membrane potentials. The

high  $I_h$  may be important for excitability of A-nociceptors (responsible for sharp/pricking-type pain) and  $A\alpha/\beta$ -LTMs (tactile sensations and proprioception). Underlying HCN expression in these subgroups therefore needs to be determined. Altered  $I_h$  expression and/or properties (e.g. in chronic/pathological pain states) may influence both nociceptor and LTM excitability.

(Resubmitted 7 June 2012; accepted after revision 28 June 2012; first published online 2 July 2012)

**Corresponding author** S. N. Lawson: School of Physiology and Pharmacology, Medical Sciences Building, University of Bristol, Bristol BS8 1TD, UK. Email: sally.lawson@bristol.ac.uk

**Abbreviations** AP, action potential; CV, conduction velocity; DRG, dorsal root ganglion; dSEVC, discontinuous single electrode voltage clamp; DCC, discontinuous current clamp; F, field; G, guard hair; HCN, hyperpolarization-activated cyclic nucleotide-gated channel; HTM, high threshold mechanoreceptor;  $I_{deac}$ , deactivation current;  $I_h$ , hyperpolarisation-activated current;  $I_{ini}$ , initial (instantaneous) inward current;  $I_{ss}$ , steady state current; LTM, low threshold mechanoreceptor; MSA, muscle spindle afferent; NT3, neurotrophin 3; RA, rapidly adapting; SA, slowly adapting.

## Introduction

The hyperpolarisation-activated current ( $I_h$ ), that generates inward current at hyperpolarised potentials was first described in cardiac pacemaker cells (DiFrancesco & Ojeda, 1980), and was subsequently identified in a variety of neurons including primary afferent dorsal root ganglion (DRG) neurons (Mayer & Westbrook, 1983; Bader & Bertrand, 1984; Crepel & Penit-Soria, 1986; Maccaferri *et al.* 1993). In A-fibre neurons *in vivo*, a membrane voltage, evoked by hyperpolarising current, had properties later associated with  $I_h$  (Harper & Lawson, 1985), and  $I_h$  was described in mainly medium-large cultured DRG neurons (Chaplan *et al.* 2003; Yao *et al.* 2003; Tu *et al.* 2004).  $I_h$  was also recorded in a few acutely isolated DRG small neurons (Scroggs *et al.* 1994; Cardenas *et al.* 1999).  $I_h$  contributes to electrophysiological properties such as membrane potential ( $E_m$ ) (Tu *et al.* 2004), adaptation (Spain *et al.* 1987; Takigawa *et al.* 1998), and after-hyperpolarisation (McCormick & Pape, 1990; Womble & Moises, 1993) of CNS and DRG neurons and thus is likely to influence membrane excitability.

$I_h$  in DRG neurons has been implicated in chronic pain (Chaplan *et al.* 2003; Yao *et al.* 2003; Tu *et al.* 2004; Momin *et al.* 2008; Emery *et al.* 2011). Regarding the types of neurons that express it, a general finding is that larger, or faster conducting, DRG or nodose ganglion neurons express greater  $I_h$ , and with faster activation times than smaller, more slowly conducting neurons (Villiere & McLachlan, 1996; Doan & Kunze, 1999; Hogan & Poroli, 2008; Kouranova *et al.* 2008). However, although DRG neuron soma size is related to fibre conduction velocity (CV) (Harper & Lawson, 1985), it provides only limited guidance as to sensory properties, because all ranges of cell size and CVs (C, A $\delta$  and A $\alpha/\beta$ ) include both nociceptors and low threshold mechanoreceptors (LTMs) (Fang *et al.* 2002; Djouhri *et al.* 2003). Therefore none of the above information indicates whether  $I_h$  expression is related to LTMs *versus* nociceptors, or to CV only.

The channels underlying  $I_h$  are the hyperpolarisation-activated, cyclic nucleotide-gated family of four non-selective cation (HCN1–4) channels. HCN1 has the fastest activation rates, followed in order by HCN2, HCN3 and HCN4 (Moosmang *et al.* 2001).  $I_h$  activation rates that differ in different sensory neuronal subgroups will suggest the isoform or isoforms likely to contribute to their  $I_h$ . While  $I_h$  activation is faster in very large DRG neurons than in small neurons (e.g. Kouranova *et al.* 2008), activation rates have not been studied in relation to sensory properties.

We therefore investigated  $I_h$  *in vivo* in identified nociceptive and LTM neurons in L4–L6 DRGs. Recordings were made intracellularly in anaesthetised rats and their sensory properties were identified. Discontinuous single electrode voltage clamp was then used to record  $I_h$  and examine its magnitude, density and biophysical properties, including reversal potential, fast and slow activation rates ( $\tau$  values) and half-activation potential ( $V_{0.5}$ ). We explored whether these variables were related to sensory properties or CVs. The  $\tau$  and  $V_{0.5}$  values allowed us to predict which HCN isoforms contribute to  $I_h$  in different neuronal subgroups.

## Methods

### Animal preparation

Experimental procedures were under UK Home Office guidelines. Rats were killed at the end of experiments with an anaesthetic overdose. For details of rat preparation for electrophysiological recording see Fang *et al.* (2002, 2005, 2006) and Djouhri *et al.* (2003). Female Wistar rats (150–180 g) were anaesthetized with sodium pentobarbital (70–80 mg kg<sup>-1</sup>, i.p.) to produce deep anaesthesia with no reflex withdrawal to pinch of the forepaw. Fur on the left hindlimb was clipped short. A tracheotomy enabled artificial ventilation and monitoring of end-tidal

CO<sub>2</sub>. The right carotid artery and right external jugular vein were cannulated for blood pressure monitoring and i.v. injections. Throughout the experiment, further anaesthetic (10 mg kg<sup>-1</sup>, i.v.) was administered hourly. The left L4, L5 and sometimes L6 DRGs and their dorsal roots were exposed. A pool for liquid paraffin was created with dental impression paste (Xantopren VL plus, Hanau, Germany); this was maintained at ~30°C (28.5–32°C). The core temperature was 35 ± 0.5°C.

The DRG under study was slightly raised by a small silver platform, to improve recording stability; its dorsal root was cut near the spinal cord entry and placed over a pair of bipolar platinum stimulating electrodes within the liquid paraffin. The left hindpaw was fixed with the dorsal hairy surface downwards with superglue to a platform to improve stability during search for receptive fields; the plantar surface was exposed upwards for sensory testing. Blood pressure (~80–100 mmHg) remained stable throughout experiments, indicating deep anaesthesia. Just prior to recording, muscle relaxant (pancuronium bromide, 1 mg kg<sup>-1</sup> i.v.) was administered, with repeat doses approximately hourly. All pancuronium doses were accompanied by the hourly anaesthetic (10 mg kg<sup>-1</sup> i.v.).

### Intracellular recordings

Borosilicate microelectrodes were filled with 3 M KCl (40–90 MΩ). Neurons were penetrated by advancing the microelectrode in 1 μm steps and applying a small capacitance buzz until an  $E_m$  was recorded. Once a stable  $E_m$  was obtained, the dorsal root was stimulated with a rectangular pulse (0.03 ms duration for A-fibre neurons or 0.3 ms for C-fibre neurons) with a gradually increasing voltage until a somatic action potential (AP) was evoked (threshold). A stimulus twice threshold for A-neurons or suprathreshold for C-neurons was used to evoke somatic APs that were recorded for offline analysis. Recordings were amplified (Axoclamp 2A, Molecular Devices, Sunnyvale, CA, USA), digitized (1401, at 40 kHz, Cambridge Electronic Design (CED), Cambridge, UK) and recorded by a PC running CED Spike2 v. 4–6.

### Conduction velocity (CV)

The conduction distance between the cathode and the recorded DRG neuron, divided by latency (including utilization time) provided CV as previously described (Djoughri & Lawson, 2001). CV classes were C (<1.0 m s<sup>-1</sup>), Aδ (1.5 to 6.5 m s<sup>-1</sup>) or Aα/β (>6.5 m s<sup>-1</sup>); these boundaries had been determined with dorsal root compound action potentials under the same conditions (temperature, sex, rat weight) (Fang *et al.* 2002).

### Identification of sensory properties

Hand-held stimulators were used to evaluate sensory properties of each recorded DRG neuron. These were applied to the hindlimb and flank. We have published full details of combinations of stimuli and responses to these, necessary to identify different classes of neuron (Lawson *et al.* 1997; Djoughri *et al.* 1998; Parekh *et al.* 2010). Non-noxious mechanical stimuli (including light touch, brushing, tapping, stretching and light pressure) were applied first. Low-threshold mechanoreceptive (LTM) neurons responded to these stimuli. If the neuron did not respond, noxious mechanical stimuli, initially stronger pressure, then pricking (needle), pinching or squeezing (flat or toothed forceps) were applied. Responses to cooling with a brief localized spray of ethyl chloride were tested. Only mechanical nociceptors with superficial receptive fields were tested with heat (hot water >50°C). Nociceptors were neurons that responded only to noxious stimuli; they included high-threshold mechanoreceptors (HTMs), polymodal mechano-heat units, or mechano-cold units. Mechano-heat and mechano-cold units thus had superficial (probably epidermal) receptive fields for mechanical stimuli (responding to pricking or fine superficial pinch). HTMs had superficial or non-superficial (sometimes deep, subcutaneous) receptive fields; those with non-superficial receptive fields were classed as HTMs by default, due to no thermal testing. Cooling units responded only to cooling.

The sensory properties of neurons in each CV group are summarised below. LTMs and nociceptors were in all CV groups. Neurons with Aα/β-fibres included muscle spindle afferents (MSAs), cutaneous LTMs and Aβ-nociceptors. Cutaneous Aα/β-LTMs included rapidly adapting (RA) and slowly adapting (SA) units. RA units responded best to moving stimuli: in glabrous skin they were glabrous RA and in hairy skin they were guard hair (G) or field (F) units. SA units showed sustained firing to sustained gentle pressure. MSAs responded to gentle pressure over the muscle and to vibration (100–250 Hz) and had a receptive field that did not move with the skin if that was moved, showing them to be subcutaneous. Many MSAs showed ongoing firing because of muscle stretch due to (a) extension of the hindlimb and (b) use of muscle relaxant (see Parekh *et al.* 2010). Nociceptors had Aβ, Aδ or C-fibre CVs. Most Aδ-LTMs were D hair units with large receptive fields that were very sensitive to slow movement of hair, skin stretch and cooling. One such unit was included with Aδ-LTMs despite having a CV of 7.13 m s<sup>-1</sup>; a few D hair-type units commonly fall slightly above the Aδ CV range (Djoughri & Lawson, 2004). C-LTMs were sensitive to cooling and very slow movement across skin. A-fibre nociceptors were HTMs with superficial or deep receptive fields. A subclass of Aβ-nociceptors that fired in response to moderate pressure

but fired more with noxious pressure or pinch, were classed as moderate pressure nociceptors. C-nociceptor subtypes were superficial and deep HTMs, and superficial mechano-heat (polymodal) and mechano-cold units.

Unresponsive neurons failed to respond to all the above mechanical stimuli. Those with C- or A $\delta$ -fibre CVs with typical nociceptor action potential durations, i.e. relatively broad often with a falling-phase inflection, and with a long afterhyperpolarisation (Lawson, 2002; Fang *et al.* 2005), were designated 'nociceptor-type' neurons and included in the nociceptor groups. They are indicated on scatterplots with star symbols (Figs 2–4). No unresponsive A $\alpha$ / $\beta$ -units were included.

### In vivo $I_h$ measurement

After AP recording and identification of sensory properties, discontinuous single electrode voltage clamp (dSEVC) was performed to record somatic  $I_h$ , after balancing the bridge, and neutralizing electrode capacitance in discontinuous current clamp (DCC) mode. Neurons were held at resting  $E_m$  if this was between  $-50$  and  $-60$  mV; otherwise they were held at  $-60$  mV. To elicit  $I_h$ , neurons were hyperpolarised for 1 s from holding potential in steps of  $-10$  mV to reach  $-130$  mV (Fig. 1A), with a 5 s interval between test pulses. Another inward current that could also be evoked by these hyperpolarizing voltage steps is the inward rectifier K<sup>+</sup> current, but this current is unlikely to have contributed to the recorded current because the inward rectifier K<sup>+</sup> current is a) blocked by sodium pentobarbitone (Gibbons *et al.* 1996), the anaesthetic used here; b) has fast, almost instantaneous activation kinetics so it will be a component of the voltage-independent leak 'pedestal' current and c) is found only in <15% of somata of small and large DRG neurons (Scroggs *et al.* 1994).

The Axoclamp 2A amplifier with X0.1L headstage had a switching frequency of 8 kHz; data were recorded by the CED 1401 at 20 kHz, and filtered at 1 kHz. Neither  $I_h$  amplitude nor  $I_h$  density differed between holding potentials of  $-50$  and  $-60$  mV when measured at  $-100$  mV test potentials in six neurons (paired  $t$  test;  $P > 0.2$ , data not shown). The recorded current had the characteristics of  $I_h$  (see Biel *et al.* 2009); it was hyperpolarisation activated, showed a voltage sag in response to step hyperpolarising currents (time-dependent rectification), was blocked with ZD7288 (see below) and had appropriate reversal potentials (see Results).

### $I_h$ , cell capacitance and $I_h$ density

For each testing potential an initial (instantaneous) inward current ( $I_{ini}$ ) was measured 12–15 ms after the start of each

voltage command to avoid the influence of capacitive artifacts (Rodrigues & Oertel, 2006) and a steady state current ( $I_{ss}$ ; Fig. 1A) was measured when the current was fully activated, i.e. during the last 0.2 s of each 1 s voltage step.  $I_h$  was measured as in Fig. 1A.

Under DCC mode, a series of negative current injections ( $-0.5$  to  $-4$  nA with a step of  $-0.5$  nA, 100 ms duration) was applied (see Fig. 1B). The input resistance ( $R_i$ ) for the neuron was calculated from the injected current and the maximum change in potential. The section from 20% to 80% of the onset of the potential change was fitted by a single exponential function to yield the membrane time constant ( $\tau_m$ ). Cell capacitance ( $C_i$ ) for each neuron was calculated from  $\tau_m$  divided by  $R_i$ , and then averaged for all test currents.  $I_h$  density was calculated by dividing  $I_h$  (at  $-100$  mV) by  $C_i$ .

The time constants for  $I_h$  activation ( $\tau$  values) current traces (example in Fig. 1A) were fitted offline to determine  $\tau$  values for test potentials of  $-100 \pm 5$  mV using Prism 5 (Graphpad, San Diego, CA, USA). In each case the first 500 ms after the onset of  $I_h$  was fitted with both a single and a double (least square error) exponential equation. The resulting single and double fits were compared and the best fit chosen (the null hypothesis was single exponential fit is better,  $P < 0.0001$ ). In the majority of neurons (56/59),  $r^2$  was  $>0.95$  with a significantly better fit with a double exponential. Because the temperature of our recorded neurons was  $28.5$ – $32^\circ\text{C}$  (mostly  $29.5$ – $30.5^\circ\text{C}$ ), we adjusted fast and slow  $\tau$  values using a  $Q_{10}$  of 3 (see below) to correct to  $30^\circ\text{C}$ . All patterns reported below were similar if the raw data were used, although the latter resulted in slightly more scatter.

### Comparison with published $\tau$ values at $-100$ mV for HCN isoforms

Fast and slow  $\tau$  values vary considerably with voltage and temperature. Our data are at  $\sim 30^\circ\text{C}$ , while most studies on HCN isoforms were at room temperature. We therefore derived estimates of fast and slow  $\tau$  ranges at  $-100$  mV from published data for heterologously expressed HCN channels (Ishii *et al.* 1999; Ulens & Tytgat, 2001; Chen *et al.* 2001) to compare with our  $30^\circ\text{C}$  data in Figs 3 and 4.

The  $Q_{10}$  values of 3 for  $I_h$  in large sensory neurons (Pena *et al.* 2006) and 4.5 in whole CNS neurons (Magee, 1998) were both used.  $Q_{10}$  values of 3 and 4 have also been used for  $I_h$  in transfected heterologous cells (Santoro & Tibbs, 1999). By using the range of  $Q_{10}$  (3–4.5) we provide a full range of likely values for both fast and slow  $\tau$  values. We made the assumption that (a) activation energy is unchanged over the  $20$ – $30^\circ\text{C}$  range and (b) that  $I_h$   $Q_{10}$  falls between 3 and 4.5 in different neuronal groups.



### Effect of ZD7288

In the last functionally identified neuron of three experiments, the effect of  $I_h$  blockade by ZD7288 was investigated.  $I_h$  and voltage sag were recorded (Fig. 1C and E), then ZD7288 (6 mg kg<sup>-1</sup>, i.v., 5 mg ml<sup>-1</sup> in 0.9% saline i.v. at 35°C) was immediately administered, and  $I_h$  and voltage sag were recorded again ~8 min later; both were substantially reduced see Fig. 1C–E and Results.

### I–V relationship and reversal potential ( $V_{rev}$ )

$I_h$  was fully activated by a prepulse to –130 mV for 1 s and then deactivated by a series of 1 s depolarization steps from –120 to –60 mV, at –10 mV increments (see Fig. 1F). The remaining  $I_h$  current immediately after the instantaneous current step in response to depolarisation (arrow Fig. 1F) was plotted against  $E_m$ .  $V_{rev}$  was the intersection of the line with the X-axis (Fig. 1G).

### Half-activation potential ( $V_{0.5}$ )

Instantaneous tail currents (Fig. 4A) were generated by switching to –130 mV after 1 s hyperpolarising pre-pulses of voltages between –50 and –130 mV, at 10 mV increments (e.g. double headed arrow, Fig. 4A). They were normalized to the maximum value obtained with the –130 mV prepulse and plotted against the corresponding prepulse voltages to yield activation curves (see Fig. 4B).  $V_{0.5}$  values were obtained by fitting the curve with a Boltzmann equation.

### Statistics

All statistical comparison of subgroups of neurons were non-parametric due to (a) small numbers per group and/or (b) data for one or more groups failing the normality test. Where all neurons are grouped together, means  $\pm$  SEM are shown where these data were normally distributed. Thus comparison of medians of data in scatterplots (Figs 2–4) were with the Kruskal–Wallis test for three or more groups (continuous lines indicate groups tested), with Dunn's *post hoc* test between all combinations of tested groups. The Mann–Whitney test (dashed lines) was used for comparison between medians of two groups. Correlations were examined with linear regression analysis with  $r^2$  values; significant regression lines are on graphs (Figs 1G, 3E and F and 4D and E). In Fig. 3C and D, lines were not shown because these were double log plots. Non-parametric Spearman correlations (with Spearman's correlation coefficient,  $r_s$ , where significant) were tested for data on Fig. 2C and D. All tests were performed with Prism 5 (GraphPad Software, La Jolla, CA, USA). Tests were two-tailed and  $P < 0.05$  was considered statistically significant.

## Results

### Identification of $I_h$

The recorded current had the following characteristics confirming its identity as  $I_h$ : (a) it was activated by hyperpolarisation from  $E_m$  (~–50 to –60 mV), see Fig. 1A; (b) in neurons with  $I_h$  amplitude  $\geq -0.5$  nA (at a –100 mV test potential), responses to hyperpolarising current injection showed  $I_h$ -induced depolarisation (voltage sag; Fig. 1B); (c) for all tested neurons with  $I_h \geq -0.5$  nA, the median reversal potential ( $V_{rev}$ ) of –31 mV, and mean  $V_{0.5}$  of –81 mV (described below) were similar to those previously reported for  $I_h$  in dissociated/cultured DRG neurons ( $V_{rev}$  –22 to –29 mV,  $V_{0.5}$  –72 to –94 mV) (Scroggs *et al.* 1994; Wang *et al.* 1997; Yao *et al.* 2003; Chaplan *et al.* 2003; Tu *et al.* 2004); and (d) 8 min after administration of the  $I_h$  blocker ZD7288 (6 mg kg<sup>-1</sup> i.v.), the current was reduced (by >80%) with suppression of the voltage sag in the two MSAs and the one  $A\alpha/\beta$  LTM SA neuron tested (Fig. 1C–E). Thus in neurons with  $I_h \geq -0.5$  nA we are confident that the current is  $I_h$ , with little or no contamination with other currents.

However, with the dSEVC method, there are higher noise levels than with whole cell patch recordings. In neurons with a measured current  $\leq -0.5$  nA the signal to noise levels were sometimes too low to be able to exclude any contamination with currents other than  $I_h$  (see Methods). Thus, although we report currents smaller than –0.5 nA, all the more exacting analyses of  $I_h$  properties (including activation rates and  $V_{0.5}$ ) were limited to neurons with  $I_h \geq -0.5$  nA.

### $I_h$ reversal potential ( $V_{rev}$ )

I–V plots were generated in 44  $I_h$ -expressing neurons (Fig. 1F and G).  $V_{rev}$  did not differ significantly between the A-fibre neuron groups compared. Median values were as follows: MSAs –31.7 mV,  $A\alpha/\beta$  cutaneous LTMs –30.0 mV,  $A\beta$ -nociceptors –30.0 mV,  $A\delta$ -nociceptors –36.0 mV, and the C-neuron –41.0 mV. For all neurons together, the median  $V_{rev}$  was –30.5 mV.

### $I_h$ expression in functionally identified DRG neurons

In 40 rats, dSEVC was performed on 117 neurons with clearly identified sensory properties. Numbers of different types of neurons are shown in Fig. 2A. Of the  $A\alpha/\beta$ -nociceptors, 11 were moderate pressure receptors, but in none of the measures in this paper did they show differences from other  $A\beta$ -nociceptors.

### $I_h$ and $I_h$ density

$I_h$  and  $I_h$  density ( $I_h/C_i$  expressed as pA pF<sup>-1</sup>) of DRG neurons at –100 mV (Fig. 1A, B and Methods) are plotted

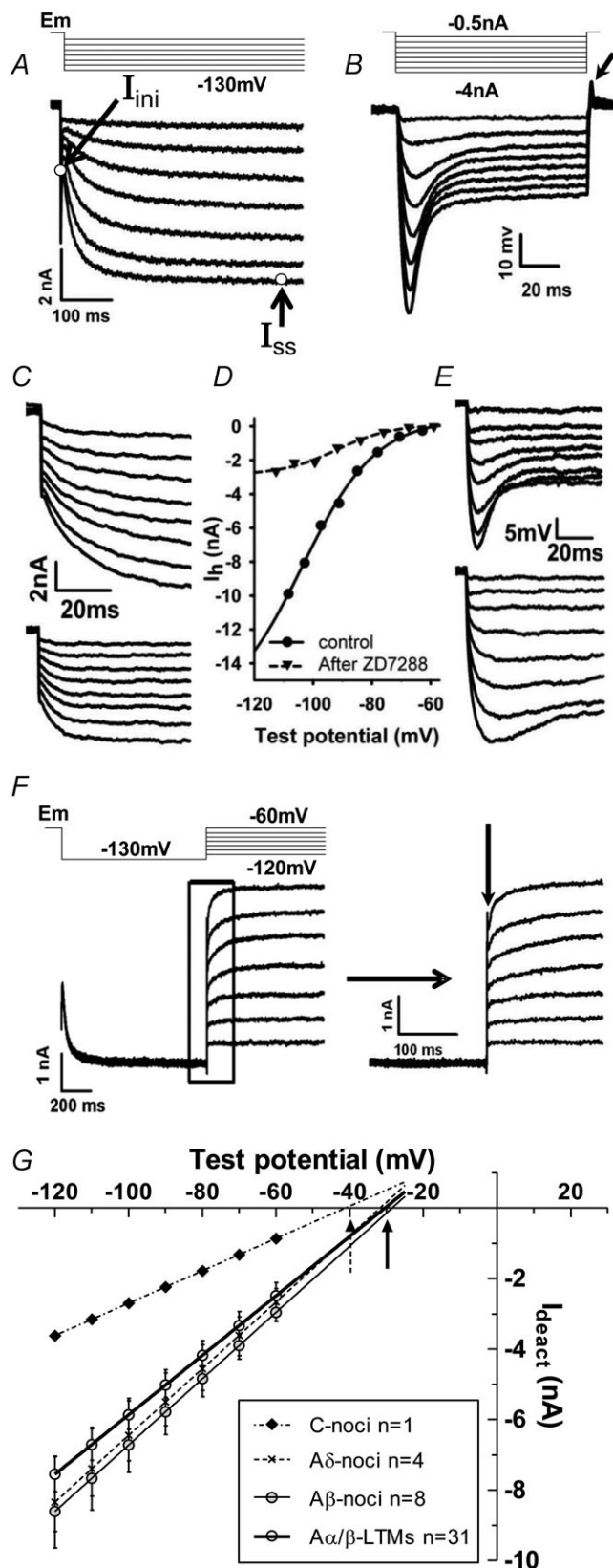


**Figure 1.**  $I_h$  measurement and characterisation

*A*, in voltage-clamp mode  $I_h$  in an  $A\alpha/\beta$ -HTM neuron recorded *in vivo*, and activated by hyperpolarisation steps from  $E_m$  ( $-50$  to

in Fig. 2*A* and *B*. Median  $I_h$  and  $I_h$  densities show similar distributions and similar patterns of significance between groups (Fig. 2, Table 1).  $I_h$  magnitude was at least  $-0.5$  nA (dotted line, Fig. 2*A*) in 31% of C-neurons, 78% of  $A\delta$ -neurons and 97%  $A\alpha/\beta$ -neurons, consistent with reported percentages for small, medium-sized and large neurons (Tu *et al.* 2004). This percentage for  $A\alpha/\beta$ -neurons was significantly higher than for C-neurons ( $P < 0.05$ ,  $\chi^2$  test). Median  $I_h$  and  $I_h$  density were significantly greater in  $A\alpha/\beta$ -neurons than in  $A\delta$ -neurons, or all C-neurons (Fig. 2, medians in Table 1).

C-nociceptor-type neurons had the lowest  $I_h$  and  $I_h$  density of any group. C-nociceptors ( $n = 4$ ) had low and similar  $I_h$  and  $I_h$  density ( $-0.11$  nA,  $-2.1$  pA pF $^{-1}$ ) to the C-silent units ( $-0.3$  nA,  $-6.1$  pA pF $^{-1}$ ). The neuron with the highest values ( $-1.15$  nA,  $-14.4$  pA pF $^{-1}$ ) was a borderline C/ $A\delta$  neuron ( $CV = 1.04$  m s $^{-1}$ ). The overall  $I_h$  and  $I_h$  density for all these neurons was  $-0.26$  nA and  $-5$  pA pF $^{-1}$ .  $A\delta$ -nociceptors had similar  $I_h$  and  $I_h$  density to  $A\delta$  LTMs, and intermediate between C- and  $A\alpha/\beta$ -neurons.  $A\alpha/\beta$ -nociceptors had  $I_h$  and  $I_h$  density similar to  $A\alpha/\beta$ -cutaneous LTMs. There was no significant difference in  $I_h$  magnitude or  $I_h$  density (Fig. 2*A* and *B*) between nociceptive and non-nociceptive neurons in any of the three CV groups ( $P > 0.1$  in all cases). The median  $I_h$  magnitude in the 11 moderate pressure nociceptors did not differ from that of other  $A\beta$ -nociceptors (data not shown); they were therefore included within the  $A\beta$ -nociceptor group throughout. MSA neurons had the highest  $I_h$  and  $I_h$  density significantly greater than cutaneous  $A\alpha/\beta$ -LTMs ( $-4.6$  nA and  $32.5$  pA pF $^{-1}$ , Fig. 2) and than all other  $A\alpha/\beta$ -neurons. MSAs also had the highest median  $I_h$  and  $I_h$  density, highly significantly greater than for all other neurons recorded ( $P < 0.0001$  for both, Mann–Whitney test). Only one C-cooling unit

$-60$  mV; in this case  $-55$  mV) to  $-130$  mV for 1 s. Open circles in the lowest  $I_h$  trace indicates the initial ( $I_{ini}$ ) and steady state ( $I_{ss}$ ) of  $I_h$  at  $-130$  mV.  $I_h$  amplitude at  $-130$  mV was the difference between  $I_{ss}$  and  $I_{ini}$ . *B*, in current-clamp mode, a series of hyperpolarising current injections (100 ms duration, step  $-0.5$  nA) evoked a hyperpolarisation followed by a set of  $I_h$ -induced depolarising voltage sags. The arrow shows a rebound overshoot at the end of the current injection. *C*,  $I_h$  traces from an MSA before (upper) and after (lower)  $\sim 8$  min administration of ZD7288. *D*, Boltzmann fits for  $I_h$  traces in *C*; approximately 90% of  $I_h$  at  $-100$  mV was blocked. *E*, in the same cell,  $I_h$ -induced depolarisation (sag) (upper) was also partially blocked by ZD7288 (lower). *F*, top:  $V_{rev}$  measurement protocol and below: example records of the deactivated  $I_h$  current ( $I_{deact}$ ) for  $I$ - $V$  curve plotting. Within an enlargement of the rectangle shown to the right, the vertical arrow indicates the point at which  $I_{deact}$  was measured to generate the  $I$ - $V$  plot. *G*,  $I$ - $V$  plots of  $I_{deact}$  against test potential voltages for 4 types of DRG neuron with different CV and sensory properties.  $V_{rev}$  is the intersection of the  $I$ - $V$  line with the  $X$ -axis (arrows). For all neurons together ( $n = 44$ ),  $V_{rev}$  was  $-31.5 \pm 1.1$  mV (mean  $\pm$  SEM, normally distributed).

was tested for  $I_h$ ; it showed no  $I_h$  (0 nA) and is not included in graphs or analyses.

The low median  $I_h$  density of C-nociceptors (5 pA pF<sup>-1</sup>) was similar to that of acutely isolated small DRG neurons

(3.6 pA pF<sup>-1</sup>) (Kouranova *et al.* 2008). Interestingly, the  $I_h$  density for Kouranova *et al.*'s very large (>55  $\mu$ m diameter) acutely dissociated neurons (33 pA pF<sup>-1</sup>) was closer to our median value for MSAs (32.5 pA pF<sup>-1</sup>) than

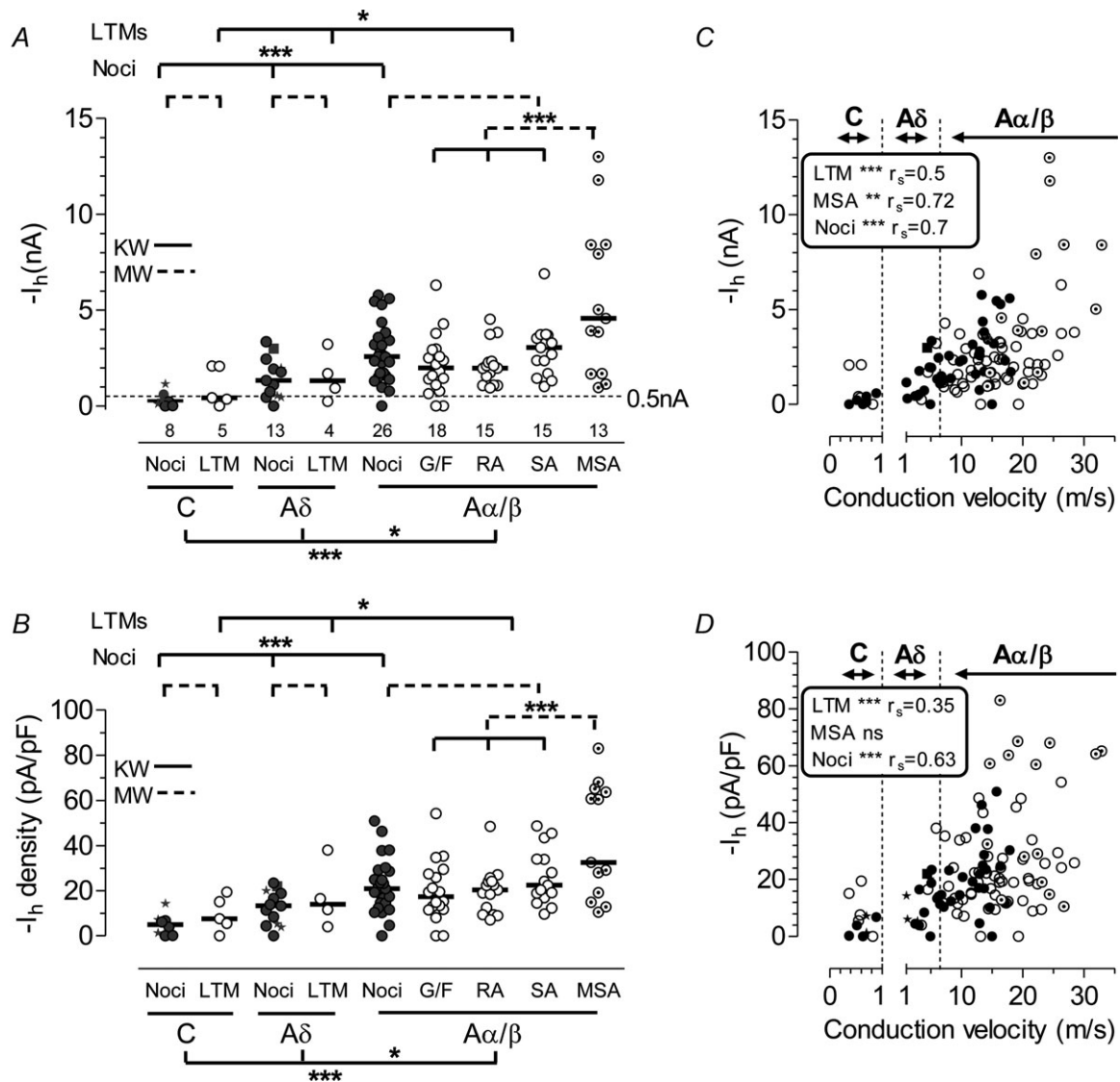


**Figure 2.**  $I_h$  versus sensory properties and CV

A,  $I_h$  magnitude in DRG neurons; each symbol represents  $I_h$  amplitude at  $-100$  mV from a neuron with identified sensory properties. Medians are shown. B:  $I_h$  density, otherwise as for A. Abbreviations: Noci: nociceptors; LTM: low threshold mechanoreceptors; G/F: G hair or field units; SA: slowly adapting; RA: rapidly adapting; MSA: muscle spindle afferents. Star symbols indicate C- and A $\delta$ -fibre unidentified nociceptor-type neurons. The filled square shows the sole A $\delta$ -mechano-cold unit. Comparisons between medians of variables were with Kruskal–Wallis (KW) test (continuous line/s) with Dunn's *post hoc* test between all groups compared (a) for all neurons (nociceptors plus LTMs) between C, A $\delta$  and A $\alpha/\beta$  neuron groups, results below graphs; then (b) between different CV groups of (i) nociceptors and (ii) LTMs (results above graphs).  $I_h$  was also compared between nociceptors and LTMs for each CV group with Mann–Whitney (MW) tests (dashed lines). Significance is indicated by \* $P < 0.05$ , \*\* $P \leq 0.01$ , \*\*\* $P \leq 0.001$ , \*\*\*\* $P \leq 0.0001$ . For the KW test, significances shown are between the groups indicated in the *post hoc* Dunn's test. C, CV versus  $I_h$ ; D, CV versus  $I_h$  density. C and D: vertical dotted lines indicate CV borderlines between C-, A $\delta$ - and A $\alpha/\beta$ -fibre neurons.  $I_h$  and  $I_h$  density were both highly correlated with CV in nociceptors (filled circles) and LTMs (open circles) and MSAs ( $I_h$  only, in C). In A–D,  $I_h$  and  $I_h$  density were highest in muscle spindle afferents (MSAs).

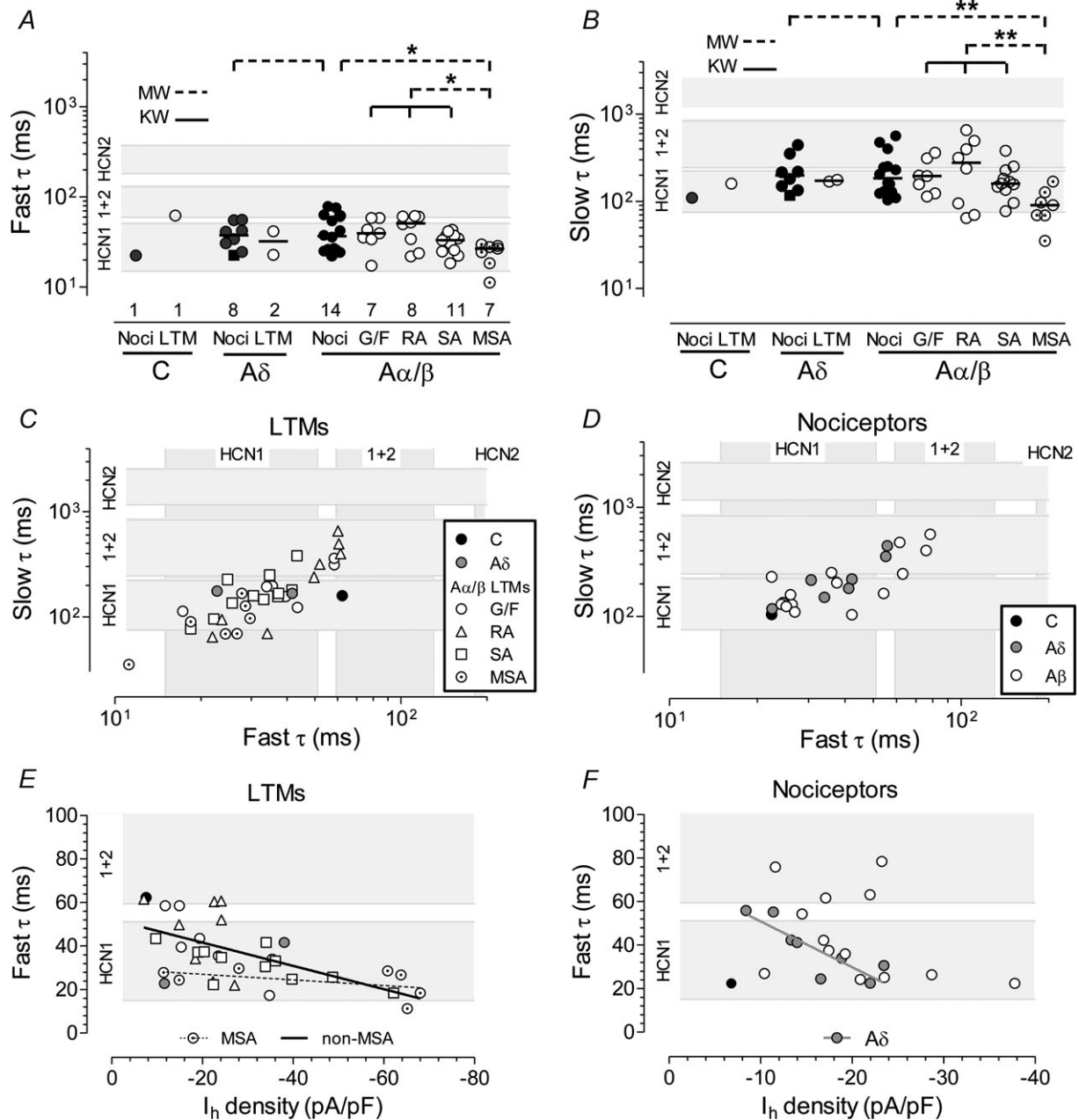


**Figure 3.**  $I_h$  activation fast and slow time constants ( $\tau$  values)

Fast and slow  $\tau$  values for each neuron were obtained from the onset of each trace of  $I_h$  (see Fig. 1A), from  $I_{ini}$  to  $I_{ss}$  (about 0.5 s) measured at  $\sim -100$  mV test potential at  $30^\circ\text{C}$  and fitted by a double exponential equation. **A** and **B**, scatterplots showing fast (**A**) and slow (**B**)  $\tau$  values plotted against sensory receptor types. The grey bands shown behind the data are to enable comparison with published fast  $\tau$  (**A**) and slow  $\tau$  (**B**) values for heterologously expressed HCN channels measured at  $-100$  mV, and recorded at room temperature. They include the likely ranges of expected values converted to  $30^\circ\text{C}$  (see Methods). Lowest grey band: HCN1; top grey band HCN2; intermediate band: HCN1+HCN2 (HCN1 co-assembled with HCN2) channels. For HCN3 and HCN4, the fast  $\tau$  ranges, derived from (Ishii *et al.* 1999; Steiber *et al.* 2005) and converted to  $30^\circ\text{C}$  are 430–554 ms for HCN3 and  $\sim 570$  to  $\sim 2635$  ms for HCN4; they fall above the Y-axis range. The square symbol in **A**, **B** and **D** is an A $\delta$ -mechanocold unit. Statistics and abbreviations as Methods and Fig. 2. In **C** and **D**, the fast  $\tau$  values are plotted against the slow  $\tau$  values for individual identified neurons for LTMs (**C**) and nociceptors (**D**). The grey bands indicate the ranges (derived as above) for fast and slow  $\tau$  values from the X- and Y-axis respectively. **C**, for all LTMs the slow  $\tau$  values are linearly correlated with the fast  $\tau$  values ( $P < 0.0001$ ,  $r^2 = 0.59$ ) and for all cutaneous A $\alpha/\beta$  LTM groups separately, RAs ( $P < 0.01$ ,  $r^2 = 0.79$ ), SA, G/F ( $P < 0.05$  for all,  $r^2 = 0.44$  and 0.68, respectively). **D**, similarly, for all nociceptors slow  $\tau$  values (continued at the bottom of page 9)



to that for non-MSA  $A\alpha/\beta$  LTM (17 pA pF<sup>-1</sup>); this is consistent with some of the largest DRG neurons being MSAs (Dobretsov *et al.* 2003; Parekh *et al.* 2010).

### $I_h$ versus CV

$I_h$  (absolute values) and  $I_h$  density were both positively correlated (Spearman's correlation) with CV in all neurons, and in both nociceptors and LTMs, as well as in subgroups of these, such as  $I_h$  in MSAs (Fig. 2C and D). MSAs (open symbols with dots) show the greatest  $I_h$  and  $I_h$  density and are some of the fastest conducting neurons (Fig. 2C and D). However, it is worth noting that in MSAs the  $I_h$  is greater than might be expected from their generally faster CVs.

This raises the question of whether  $I_h$  expression is phenotypically associated with CV in A-fibre neurons or whether  $I_h$  *per se* influences CV. CV depends not only on fibre diameter but also on the AP rate of rise. AP rise time was correlated with  $I_h$  magnitude in  $A\delta$  nociceptors ( $n = 13$ ,  $r_s = -0.6$ ,  $P < 0.05$ ) and  $A\alpha/\beta$  LTMs ( $n = 70$ ,  $r_s = -0.35$ ,  $P < 0.01$ ) (data not shown).  $I_h$  blockade by ZD7288 decreases total AP duration *in vitro* by a maximum of 10% (Tu *et al.* 2004). Furthermore, Hogan & Poroli (2008) showed in ZD7288 studies that  $I_h$  blockade did not alter CVs in  $A\delta$ - or  $A\alpha/\beta$ -neurons, which suggests little or no influence of  $I_h$  on CV in A-neurons.

### Properties of $I_h$ *in vivo* in identified neurons

Time constants of  $I_h$  activation ( $\tau$  values) were measured at  $\sim 30^\circ\text{C}$  and a test potential of  $\sim -100$  mV in 59 neurons with  $I_h$  of at least  $-0.5$  nA. The  $I_h$  activation curve for all but three neurons was fitted significantly better (see Methods) by two exponentials providing fast and slow  $\tau$  values. Numbers of neurons in each group are shown on Fig. 3A. Since most C-neurons had  $I_h < -0.5$  nA, those included are atypical of the group. For comparison with literature, grey bands on the graphs show published values measured at  $-100$  mV, converted to  $30^\circ\text{C}$  (see legend for details).

The fast  $\tau$  values range from 12 to 90 ms, with a median for all 59 neurons of 34.1 ms (Fig. 3A). The slow  $\tau$  values ranged from 35 to  $>655$  ms (Fig. 3B). The only significant difference between groups of neurons was that the MSAs had a lower median  $\tau$  than all other neurons, and than all non-MSA  $A\alpha/\beta$  neurons, both

nociceptors and cutaneous LTMs. All these significances were  $P < 0.05$  for fast  $\tau$  values and  $P < 0.01$  for slow  $\tau$  values. For all MSAs and SAs, and for most other neurons, the fast  $\tau$  values fell within the expected range for HCN1, and the rest fell within the expected range for  $\tau$  values for HCN1+HCN2 (values derived from heterologously co-expressed channels, thought to form functional heteromers; see Methods). Note that the fast  $\tau$  values for HCN3 and HCN4 are longer (slower) than for HCN2 (converted values in legend for Fig. 3), and thus much longer than fast  $\tau$  values for any of the neurons in this study. The pattern was similar for slow  $\tau$  values, but with a few more RA and A-nociceptors in the HCN1+2 range. The C-fibre nociceptor showed relatively short fast and slow  $\tau$  values, but this neuron was atypical of the majority of C-nociceptors in having an  $I_h$  of  $\geq -0.5$  nA, and thus the  $\tau$  values may also be atypical.

Note that the fast  $\tau$  values in this study fell within the range of fast  $\tau$  values in acutely dissociated DRG neurons (Kouranova *et al.* 2008) and of  $\tau$  values obtained at  $-120$  mV with a single exponential fit of  $I_h$  in neurons of acutely excised DRGs (Villiere & McLachlan, 1996), in both cases converted to  $30^\circ\text{C}$ .

There was a strong linear correlation between the fast and slow  $\tau$  values, both for LTMs (Fig. 3C) and nociceptors (Fig. 3D). For all the neuronal groups with enough values to test, there were also strong linear correlations, for  $A\alpha/\beta$  LTMs: SA, RA, G/F and for  $A\delta$ -nociceptors. Furthermore the majority of the neurons had fast and slow  $\tau$  values which fell in the expected fast and slow  $\tau$  range, respectively, for HCN1; similarly for some neurons both  $\tau$  values fell in the expected range for HCN1+2. Thus, the slow  $\tau$  showed a strong dependence on the fast  $\tau$ . The slope ( $\Delta\tau_{\text{slow}}/\Delta\tau_{\text{fast}}$ ) for all LTMs was  $7.1 \pm 1.0$  and for all nociceptors was  $6.2 \pm 0.9$ . Thus slow  $\tau$  values were  $\sim 6$ – $7$  times longer than the fast  $\tau$  values, Fig. 3C and D.

We next examined the fast  $\tau$  in relation to  $I_h$  density for different neuronal subtypes (Fig. 3E and F). We chose the fast  $\tau$  because the fast component of  $I_h$  accounts for  $>80\%$  of the current at  $-100$  mV (Chen *et al.* 2001) and we chose  $I_h$  density because this is independent of neuronal size. For the non-MSA units, the fast  $\tau$  values showed a significant negative correlation with  $I_h$  density despite a considerable scatter of fast  $\tau$  values at low  $I_h$  densities. In contrast the only LTM groups in which fast  $\tau$  values were not related to  $I_h$  density was the MSAs with similar

are linearly correlated with fast  $\tau$  values ( $P < 0.0001$ ,  $r^2 = 0.68$ ) and for  $A\delta$ -nociceptors ( $P < 0.01$ ,  $r^2 = 0.81$ ), and  $A\alpha/\beta$  ( $P < 0.001$ ,  $r^2 = 0.64$ ). In A–D,  $\tau$  axes are on a log scale so regression lines not shown. In E and F, symbols are as in C and D, respectively. In E, in all non-MSA LTMs there is a highly significant linear correlation between fast  $\tau$  values and  $I_h$  densities ( $P < 0.001$ ,  $r^2 = 0.23$ ) while for MSAs these are not significantly correlated. In F, there is no overall correlation for all nociceptors, but  $A\delta$ -nociceptors alone do show a strong correlation ( $P < 0.01$ ,  $r^2 = 0.74$ ). Many (8/13)  $A\beta$ -nociceptors fall near the same line.

fast  $\tau$  values across all  $I_h$  densities; their fast  $\tau$  values were consistent with fast  $\tau$  values for HCN1+HCN2 and much faster than for HCN3 or HCN4. The only LTM units with fast  $\tau$  values above the range for HCN1 (and consistent with HCN1+HCN2 fast  $\tau$  values) were non-MSA neurons with relatively low  $I_h$  densities. The nociceptors show a different pattern to that of the LTMs. There was no overall correlation between fast  $\tau$  values and  $I_h$  density. However the fast  $\tau$  values were strongly negatively correlated with  $I_h$  density for A $\delta$  nociceptors, with larger fast  $\tau$  values in neurons with relatively lower  $I_h$  densities. Although the A $\beta$  nociceptors showed no significant correlation overall, two-thirds of them (8/13) follow a similar pattern to the A $\delta$  neurons.

There was no correlation between  $\tau$  values (fast or slow) and CV for all neurons or for all nociceptors (not shown). For all LTMs, there was a weak linear correlation ( $P < 0.05$ ,  $r^2 = 0.13$ ).

The  $\tau$  plots (Fig. 3) indicate a predominance of cells with  $I_h$   $\tau$  values typical of HCN1. The wide range of  $\tau$  values, with a few being higher than for HCN1, suggests that HCN2 also contributes either as HCN2 channels or as HCN1+2 channels. The  $-100$  mV voltage used here (and typically in the literature) to measure  $I_h$  overestimates the HCN1 contribution because a higher proportion of HCN1 than of HCN2 is activated at this voltage (e.g. Chen *et al.* 2001). To assess whether HCN2 contributes to the  $I_h$ , we next examined the  $V_{0.5}$  values.

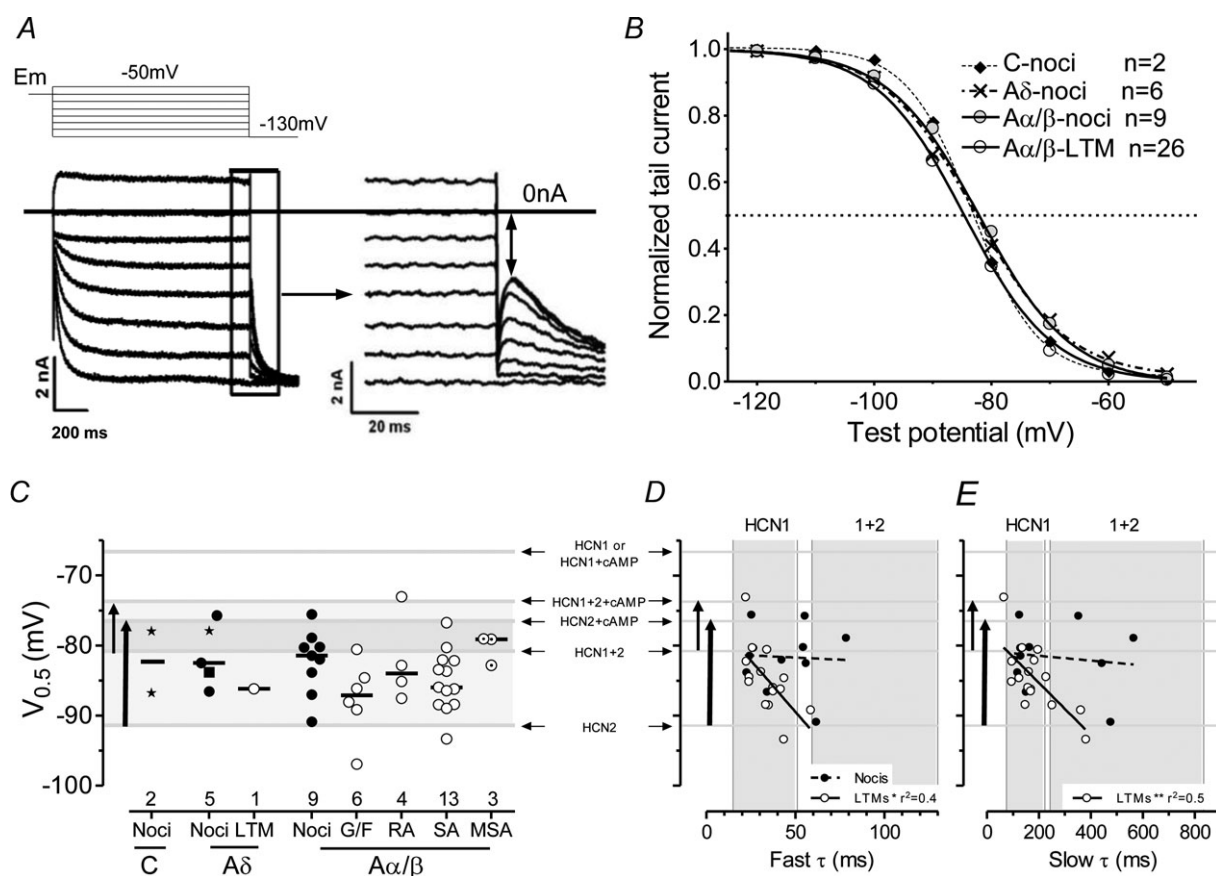


**Figure 4.**  $I_h$  half activation potential ( $V_{0.5}$ )

**A**, protocol (top) and example (lower) for activation curve plotting from hyperpolarising tail currents with (right) enlargement of the section in the rectangle. Double headed arrow illustrates where instantaneous tail currents were measured. These were normalised to the maximum tail current (after a  $-130$  mV prepulse) and plotted against prepulse magnitudes to generate activation curves. **B**, activation curves (Boltzmann fits) used to determine  $V_{0.5}$ . **C**, scatter plots for  $V_{0.5}$  for different groups of neurons. No significant differences were seen (statistical comparisons as in Fig. 2). Star symbols indicate C- and A $\delta$ -fibre unidentified nociceptor-type neurons. For more on statistics and abbreviations see Methods and Fig. 2 legend. In **C**, **D** and **E**, grey lines illustrate published  $V_{0.5}$  values for the channels and conditions indicated, the vertical arrows indicate the published  $V_{0.5}$  ranges for HCN2 from no cAMP to high cAMP, and for HCN1+HCN2 heteromeric channels from no cAMP to high cAMP. Thus top of arrows indicate high cAMP. **D**, plot of  $V_{0.5}$  against fast  $\tau$ . Grey lines and arrows as for **C**, vertical grey bands from published fast  $\tau$  values as in Fig. 3. **E** as for **D**, but for slow  $\tau$  values; vertical grey bands show published  $\tau$  values (see Fig. 2).

**Table 1. Summary for neuronal subgroups of medians values for  $I_h$ ,  $I_h$  density,  $V_{0.5}$  and  $I_h$  activation  $\tau$  values**

	<i>n</i>	$I_h$ (nA)	$I_h$ density (pA pF <sup>-1</sup> )	<i>n</i>	$V_{0.5}$ (mV)	<i>n</i>	$I_h$ $\tau$ values at -100 mV	
							fast	slow
C noci	8	0.26	5.0	2	82.4	1	22.4	109.9
C LTM	5	0.42	7.6	1	86.2	1	62.3	159.4
A $\delta$ -noci	13	1.33	13.3	5	82.5	8	34.1	197.9
A $\delta$ LTM	4	1.31	14.1			2	32.2	172.5
A $\beta$ noci	26	2.57	20.9	9	81.5	14	36.7	180.3
A $\alpha/\beta$ LTMs	61	2.35	21.3	26	84.9	36	33.9	156.8
A $\alpha/\beta$ cut LTM	48	2.22	20.4	23	86	26	34.1	174.4
A $\alpha/\beta$ SA	15	3.0	22.4	13	86	11	33.2	160
A $\alpha/\beta$ RA	15	1.98	20.4	4	84	8	50.9	277
A $\alpha/\beta$ G/F	18	1.98	17.3	6	87.1	7	39.5	194.6
A $\alpha/\beta$ MSA	13	4.6	32.5	3	79.1	7	26.7	90.2

Numbers of neurons (*n*) relate to columns to their right.  $I_h$  was recorded at  $\sim 30^\circ\text{C}$  and  $\sim -100$  mV.

### $I_h$ half-activation potential ( $V_{0.5}$ )

$V_{0.5}$  was calculated (protocol in Fig. 4A) in 43 DRG neurons with  $I_h$  greater than  $-0.5$  nA (the number of units in each group shown in Fig. 4C). The curves for different neuronal groups are very similar to each other (Fig. 4B), despite differences between published curves for heterologously expressed HCN1 and HCN2 (Santoro *et al.* 2000; Chen *et al.* 2001; Ulens & Tytgat, 2001), providing no evidence for groups of neurons in which  $I_h$  derives from only one of the two isoforms. For all neurons,  $V_{0.5}$  value and slope factors were  $-83.8 \pm 0.7$  mV and  $-7.0 \pm 0.2$  respectively (mean  $\pm$  SEM, normally distributed; Fig. 4B). The activation curves in Fig. 4B show that  $\sim 3$ – $7\%$  of  $I_h$  would be activated at an  $E_m$  of  $-60$  mV, and 2–4% at an  $E_m$  of  $-55$  mV. The neurons in this study had  $E_m$  values of  $-63 \pm 1.2$  mV (mean  $\pm$  SEM), so on average  $I_h$  would contribute to resting  $E_m$ .

Since  $I_h$  values derived from HCN1 and HCN2 channels have rather different half-activation potential ( $V_{0.5}$ ), we examined  $V_{0.5}$  for different sensory subgroups. Median  $V_{0.5}$  values for all neuronal subgroups are shown in Table 1 and Fig. 4B. The medians did not differ significantly between neurons with different sensory properties, perhaps because of the large range of  $V_{0.5}$  values within the groups. Nonetheless, the medians were (non-significantly) more depolarised for the A-nociceptors and MSAs than for A $\alpha/\beta$  cutaneous LTMs.

For comparison of these  $V_{0.5}$  values for these identified neurons with published values for HCN1 and HCN2, labelled grey lines have been added to show published values for HCN1, HCN2 and HCN1+HCN2, with or without added cAMP (Ulens & Tytgat, 2001) (for effects of cAMP on HCN2 see Discussion). Grey bands show (a) the range of values for HCN2 without cAMP (lower end of thick arrow) to high (forskolin-induced) cAMP (top of

arrow), and (b) a similar range from low to high cAMP for HCN1+HCN2 heteromer channels (thin arrow). The darker grey band is the overlap between (a) and (b). Most (74%) A $\alpha/\beta$  cutaneous LTM  $V_{0.5}$  values fell in the HCN2 band within a region associated with the presence of cAMP (Fig. 4C). Interestingly for several other groups, including A $\delta$  and A $\beta$  nociceptors and MSAs, the medians are close to the  $V_{0.5}$  values for HCN1+2. Notably, none of the  $V_{0.5}$  values approached that for HCN1 (Fig. 4C).

Because both  $\tau$  values and  $V_{0.5}$  differ for different isoforms, and because cAMP shortens HCN2  $\tau$  values and depolarises HCN2  $V_{0.5}$  values, plotting  $V_{0.5}$  against  $\tau$  values may provide further information about the likely isoforms underlying  $I_h$  in the different neurons. The pattern for fast and slow  $\tau$  values was remarkably similar (Fig. 4D and E). There was no correlation with  $V_{0.5}$  for nociceptors, while for LTMs there was a negative correlation between  $V_{0.5}$  and both fast and slow  $\tau$  values, such that  $I_h$  with longer  $\tau$  values (slower activation) had more hyperpolarised  $V_{0.5}$  values.

Overall, the above findings can be summarised as follows. The group (cutaneous LTMs) with not only HCN1-like but also the slower (HCN1+2-like)  $\tau$  values tended more to HCN2-like  $V_{0.5}$  values than other groups. MSAs and nociceptors showed a trend towards HCN1-like  $\tau$  values, and HCN1+2-like  $V_{0.5}$  values. This may suggest a greater HCN1 influence on  $I_h$  in MSAs and nociceptors and a greater HCN2 influence on  $I_h$  in A $\alpha/\beta$ -cutaneous LTMs.

## Discussion

By making intracellular recordings from DRG neurons *in vivo*, which allows identification of their sensory properties and CVs, we have determined the relationship of  $I_h$  and

its kinetics to these properties for the first time. We found positive correlations of  $I_h$  and  $I_h$  density with CV. Our findings include (a) a similar  $I_h$  magnitude in LTMs and nociceptors with similar CVs, and thus high  $I_h$  in A $\beta$ -nociceptors; (b) higher median  $I_h$  in MSAs than in all other neuronal subgroups; (c)  $I_h$  density and fast  $\tau$  were negatively correlated for all non-MSA LTMs and A $\delta$  nociceptors; and (d)  $V_{0.5}$  with fast and slow  $\tau$  values were also negatively correlated with fast and slow  $\tau$  values for all LTMs.  $I_h$  properties suggest which isoforms underlie  $I_h$ : generally, activation kinetics support HCN1 involvement while voltage-dependent activation suggests HCN2 contributions. Thus a combination of HCN1 and HCN2 contributions to  $I_h$  is likely.

### $I_h$ *in vivo* compared with *in vitro*

Most studies on heterologously expressed HCN isoforms underlying  $I_h$  were *in vitro* at room temperature; our *in vivo* study examines  $I_h$  in neurons in a physiologically preserved environment at 30°C. To enable comparisons with published studies we adjusted *in vitro* activation time constants to 30°C. The effects of anaesthetic *in vivo* are minimal (see Methods), supported by the present *in vivo*  $I_h$  magnitudes being similar to those recorded in acutely dissociated DRG neurons (Kouranova *et al.* 2008). However, values recorded from neurons in culture for longer than a few hours were lower, e.g. the maximum  $I_h$  density of 1.2 pA pF<sup>-1</sup> recorded in large neurons (>42  $\mu$ m diameter) 6–48 h after dissociation (Chaplan *et al.* 2003) was much lower than for our A $\alpha/\beta$ -neuron median (–21 pA pF<sup>-1</sup>). This suggests a loss of  $I_h$  in large neurons in culture over time, perhaps due to a trophic factor dependence of HCN channel expression. Finally, intracellular modulation may differ in the more physiological *in vivo* environment.

### $I_h$ activation time constants ( $\tau$ values) and $V_{0.5}$

The strong linear correlations between slow and fast  $\tau$  for both LTMs and nociceptors suggest that the slow  $\tau$  values are the slow components of the same channels that are responsible for the fast  $\tau$  values. The ranges of fast and slow  $\tau$  values may thus both relate to different contributions to  $I_h$  of different channel isoforms. Because of this and because of the high contribution (>80%) of the rapidly activating component to  $I_h$  for heterologously expressed HCN1 and HCN2 channels (Chen *et al.* 2001), we limit the following discussion to fast  $\tau$  values.

The  $\tau$  values for different pure isoforms are in ascending order HCN1 < HCN2 < HCN3 < HCN4 (Moosmang *et al.* 2001; Stieber *et al.* 2005). In the present study,  $I_h$  in most A-fibre DRG neurons had  $\tau$  values consistent with published values for HCN1. In a minority of neurons

the  $\tau$  values fell between the HCN1 and HCN2 ranges, much closer to HCN1 values. While this may suggest a greater contribution to  $I_h$  of HCN1 than HCN2, it is also consistent with  $I_h$  resulting from co-assembly of HCN1 and HCN2 to form HCN1+HCN2 channels (Chen *et al.* 2001) since these have  $\tau$  values between those of HCN1 and HCN2 alone, and closer to the HCN1 values (Ulens & Tytgat, 2001; Chen *et al.* 2001). There is a precedent in neurons for functional co-assembled HCN1+HCN2 channels (Ulens & Tytgat, 2001).

While the  $\tau$  values suggest a major contribution to  $I_h$  from HCN1, the  $V_{0.5}$  values strongly indicate some contribution from HCN2. This is probably explained by HCN2 having a greater influence on  $V_{0.5}$  than on  $\tau$  values, because at  $V_{0.5}$  HCN2 is more highly activated than HCN1. In contrast a higher proportion of HCN1 than of HCN2 is activated at –100 mV, the test voltage for the  $\tau$  values. However, to explore the possible role of HCN2, we need to describe the modulatory role of cAMP on HCN2 (but not HCN1) function. cAMP acting on HCN2 increases  $I_h$  magnitude, accelerates  $I_h$  activation and shifts activation towards more depolarised potentials (Kusch *et al.* 2010, 2012). In co-assembled HCN1+HCN2 channels,  $V_{0.5}$  and cAMP-dependent depolarisation of  $V_{0.5}$  were intermediate between values for these two channels but closer to HCN2 values (Ulens & Tytgat, 2001; Chen *et al.* 2001). Importantly, cAMP is likely to be present in all neurons *in vivo* but its levels may vary between groups or amongst individual neurons, depending on e.g. their level of activity. Such variable cAMP levels may profoundly affect HCN2-related  $I_h$  magnitude,  $V_{0.5}$  and activation kinetics and may partly explain the range of values we obtained.

The  $V_{0.5}$  values from –91 mV to –77 mV (most A $\alpha/\beta$ -cutaneous LTMs) are consistent with contributions from HCN2 in the presence of variable cAMP. Values of ~–82 mV (nociceptors and MSAs) can be accounted for by HCN1+HCN2 heteromeric channels in the absence (or low) cAMP or by HCN2 with high cAMP. There are no values suggestive of HCN1 alone. This raises the question of whether HCN2 alone can account for the  $I_h$  observed or whether HCN1 is also likely to contribute. From  $\tau$  values (above) it is clear that HCN1 contributes to  $I_h$ .

### Functional significance of $I_h$

The 2–7% activation of  $I_h$  at  $E_m$  (see Results) suggests some influence on resting membrane properties, but whether  $I_h$  has excitatory or inhibitory effects in sensory neurons is not shown directly by our data. However,  $I_h$  blockade reduces the number of action potentials evoked by a depolarising current pulse in A $\alpha/\beta$ -neurons in normal whole DRGs *in vitro* (Hogan & Poroli, 2008). Similarly  $I_h$  blockade shows that even low  $I_h$



magnitudes ( $<0.5$  nA) in C-neurons can be pro-excitatory in acute inflammation (Momin *et al.* 2008; Emery *et al.* 2011). Furthermore,  $I_h$  blockade decreased CFA-evoked spontaneous firing in C-nociceptors *in vivo* (Weng *et al.* 2012). The above pro-excitatory role of  $I_h$  remains to be established for different neuronal subgroups normally and in pathological pain models.

The extent of any  $I_h$  influence on excitability will depend on the  $E_m$ ,  $I_h$  magnitude, contributions of HCN1 and HCN2, depth of afterhyperpolarisation (AHP), and factors including cAMP levels. For example, a modest  $I_h$  at  $E_m$  would increase greatly during AHPs. HCN1  $V_{0.5}$  is more depolarised ( $-67$  mV). Thus, normal AHP should activate a substantial proportion of HCN1. The proportion of HCN2 that is activated would increase with even greater AHP depth and with more cAMP, since the  $V_{0.5}$  for HCN2 alone ( $-91.4$  mV) depolarises to  $\sim -76$  mV with greater cAMP. Elevated  $I_h$  during the AHP would accelerate the repolarisation, enabling faster firing. Although the above measurements relate to soma  $I_h$ , influences of  $I_h$  on action potential initiation will depend on  $E_m$  in the fibres, which is unknown.

### MSAs

Their high  $I_h$  and fast  $\tau$  values may aid the rapidity of AHP recovery (e.g. Fang *et al.* 2005), contributing to their ability to fire rapidly and/or in a sustained fashion. The MSAs having the fastest  $I_h$  activation  $\tau$  values may relate to their having the fastest action potentials and AHPs of all groups.

### A-Nociceptors

Although it was suggested (Chaplan *et al.* 2003) that  $I_h$  might contribute to pathological pain, this is the first demonstration of high  $I_h$  in A-fibre nociceptors. This may well influence their sensitivity, and thus influence the sensations associated with these neurons, including sharp pricking or stabbing pain. The high  $I_h$  we found in A $\beta$ -nociceptors may be pro-algesic. Alteration of  $I_h$  in nociceptors in chronic or pathological pain states could have profound effects on their firing thresholds or firing rates.

### Cold

$I_h$  was implicated in cold sensation in trigeminal sensory neurons (Viana *et al.* 2002). Three subgroups of DRG neurons responded to cooling in the present study. A $\alpha/\beta$ -SA units had moderately high  $I_h$ , A $\delta$  D hair units did not have  $I_h$  higher than A $\delta$  nociceptors, but the single A $\delta$  mechano-cold unit had  $I_h$  that was large and fast for the A $\delta$  group. The single C-cooling unit had undetectable

$I_h$ . More data are needed to determine whether  $I_h$  contributes to cold sensitivity in specific cooling-sensitive subgroup(s).

### Control of $I_h$

Factors controlling  $I_h$  in sensory neurons depend on the underlying HCN isoform expression. HCN1 and HCN2 have both been reported in large diameter DRG neurons (Chaplan *et al.* 2003), but not in identified subpopulations of DRG neurons. Our present results suggest contributions to  $I_h$  of HCN1 and HCN2 in A-fibre neurons. Differences in HCN expression between MSAs, A-fibre nociceptors and A $\alpha/\beta$  cutaneous LTMs could explain differences in their  $I_h$  properties.

### Conclusion

The properties of  $I_h$  recorded in A-fibre neurons could not be explained either by HCN1 alone ( $V_{0.5}$ ) or by HCN2 alone ( $\tau$  values). Variations in kinetics and voltage dependence suggest a greater influence of HCN2 in A $\alpha/\beta$ -cutaneous LTMs and greater influence of HCN1 in A-fibre nociceptors and MSAs. They are also suggestive of both channels contributing to the observed  $I_h$ . Accordingly, we suggest that there are contributions of both isoforms to  $I_h$  to varying extents in all these neuronal types. The low  $I_h$  in C-nociceptors suggests little influence on these neurons normally. The intermediate  $I_h$  levels in A $\delta$ -neurons may have intermediate effects on neuronal properties. In contrast, the very high  $I_h$  magnitudes in MSAs, and high  $I_h$  magnitudes in cutaneous LTMs and A-fibre nociceptors suggest that membrane functions of neurons in these groups may be strongly influenced by  $I_h$ .

### References

- Bader CR & Bertrand D (1984). Effect of changes in intra- and extracellular sodium on the inward (anomalous) rectification in salamander photoreceptors. *J Physiol* **347**, 611–631.
- Biel M, Wahl-Schott C, Michalakis S & Zong X (2009). Hyperpolarization-activated cation channels: from genes to function. *Physiol Rev* **89**, 847–885.
- Cardenas CG, Mar LP, Vysokanov AV, Arnold PB, Cardenas LM, Surmeier DJ & Scroggs RS (1999). Serotonergic modulation of hyperpolarization-activated current in acutely isolated rat dorsal root ganglion neurons. *J Physiol* **518**, 507–523.
- Chaplan SR, Guo HQ, Lee DH, Luo L, Liu C, Kuei C, Velumian AA, Butler MP, Brown SM & Dubin AE (2003). Neuronal hyperpolarization-activated pacemaker channels drive neuropathic pain. *J Neurosci* **23**, 1169–1178.
- Chen S, Wang J & Siegelbaum SA (2001). Properties of hyperpolarization-activated pacemaker current defined by coassembly of HCN1 and HCN2 subunits and basal modulation by cyclic nucleotide. *J Gen Physiol* **117**, 491–504.

- Crepel F & Penit-Soria J (1986). Inward rectification and low threshold calcium conductance in rat cerebellar Purkinje cells. An *in vitro* study. *J Physiol* **372**, 1–23.
- DiFrancesco D & Ojeda C (1980). Properties of the current  $I_h$  in the sino-atrial node of the rabbit compared with those of the current  $I_K$  in Purkinje fibres. *J Physiol* **308**, 353–367.
- Djoughri L, Bleazard L & Lawson SN (1998). Association of somatic action potential shape with sensory receptive properties in guinea-pig dorsal root ganglion neurones. *J Physiol* **513**, 857–872.
- Djoughri L, Fang X, Okuse K, Wood JN, Berry CM & Lawson S (2003). The TTX-resistant sodium channel Nav1.8 (SNS/PN3): expression and correlation with membrane properties in rat nociceptive primary afferent neurons. *J Physiol* **550**, 739–752.
- Djoughri L & Lawson S. N. (2001). Differences in the size of the somatic action potential overshoot between nociceptive and non-nociceptive dorsal root ganglion neurones in the guinea-pig. *Neuroscience* **108**, 479–491.
- Djoughri L & Lawson SN (2004). A $\beta$ -Fiber nociceptive primary afferent neurons: a review of incidence and properties in relation to other afferent A-fiber neurons in mammals. *Brain Res Brain Res Rev* **46**, 131–145.
- Doan TN & Kunze DL (1999). Contribution of the hyperpolarization-activated current to the resting membrane potential of rat nodose sensory neurons. *J Physiol* **514**, 125–138.
- Dobretsov M, Hastings SL, Sims TJ, Stimers JR & Romanovsky D (2003). Stretch receptor-associated expression of alpha 3 isoform of the Na<sup>+</sup>,K<sup>+</sup>-ATPase in rat peripheral nervous system. *Neuroscience* **116**, 1069–1080.
- Emery, E. C., Young, G. T., Berrococo, E. M., Chen, L., & McNaughton, P. A. (2011). HCN2 ion channels play a central role in inflammatory and neuropathic pain. *Science* **333**, 1462–1466.
- Fang X, Djoughri L, Black JA, Dib-Hajj SD, Waxman SG & Lawson SN (2002). The presence and role of the tetrodotoxin-resistant sodium channel Na<sub>v</sub>1.9 (NaN) in nociceptive primary afferent neurons. *J Neurosci* **22**, 7425–7433.
- Fang X, Djoughri L, McMullan S, Berry C, Okuse K, Waxman SG & Lawson SN (2005). trkA is expressed in nociceptive neurons and influences electrophysiological properties via Nav1.8 expression in rapidly conducting nociceptors. *J Neurosci* **25**, 4868–4878.
- Fang X, Djoughri L, McMullan S, Berry C, Waxman SG, Okuse K & Lawson SN (2006). Intense isolectin-B4 binding in rat dorsal root ganglion neurons distinguishes C-fiber nociceptors with broad action potentials and high Nav1.9 expression. *J Neurosci* **26**, 7281–7292.
- Gibbons SJ, Nunez-Hernandez R, Maze G & Harrison NL (1996). Inhibition of a fast inwardly rectifying potassium conductance by barbiturates. *Anesth Analg* **82**, 1242–1246.
- Harper AA & Lawson SN (1985). Conduction velocity is related to morphological cell type in rat dorsal root ganglion neurones. *J Physiol* **359**, 31–46.
- Hogan QH & Poroli M (2008). Hyperpolarization-activated current ( $I_h$ ) contributes to excitability of primary sensory neurons in rats. *Brain Res* **1207**, 102–110.
- Ishii TM, Takano M, Xie LH, Noma A & Ohmori H (1999). Molecular characterization of the hyperpolarization-activated cation channel in rabbit heart sinoatrial node. *J Biol Chem* **274**, 12835–12839.
- Kouranova EV, Strassle BW, Ring RH, Bowlby MR & Vasilyev DV (2008). Hyperpolarization-activated cyclic nucleotide-gated channel mRNA and protein expression in large versus small diameter dorsal root ganglion neurons: correlation with hyperpolarization-activated current gating. *Neuroscience* **153**, 1008–1019.
- Kusch, J., Biskup, C., Thon, S., Schulz, E., Nache, V., Zimmer, T., Schwede, F., & Benndorf, K. (2010). Interdependence of receptor activation and ligand binding in HCN2 pacemaker channels. *Neuron* **67**, 75–85.
- Kusch, J., Thon, S., Schulz, E., Biskup, C., Nache, V., Zimmer, T., Seifert, R., Schwede, F., & Benndorf, K. (2012). How subunits cooperate in cAMP-induced activation of homotetrameric HCN2 channels. *Nat. Chem. Biol.* **8**, 162–169.
- Lawson SN, Crepps BA & Perl ER (1997). Relationship of substance P to afferent characteristics of dorsal root ganglion neurones in guinea-pig. *J Physiol* **505**, 177–191.
- Lawson, S. N. (2002). Phenotype and function of somatic primary afferent nociceptive neurones with C-, Delta- or Aalpha/beta-fibres. *Exp. Physiol* **87**, 239–244.
- Maccaferri G, Mangoni M, Lazzari A & DiFrancesco D (1993). Properties of the hyperpolarization-activated current in rat hippocampal CA1 pyramidal cells. *J Neurophysiol* **69**, 2129–2136.
- Magee JC (1998). Dendritic hyperpolarization-activated currents modify the integrative properties of hippocampal CA1 pyramidal neurons. *J. Neurosci* **18**, 7613–7624.
- Mayer ML & Westbrook GL (1983). A voltage-clamp analysis of inward (anomalous) rectification in mouse spinal sensory ganglion neurones. *J Physiol* **340**, 19–45.
- McCormick DA & Pape HC (1990). Properties of a hyperpolarization-activated cation current and its role in rhythmic oscillation in thalamic relay neurones. *J Physiol* **431**, 291–318.
- Momin, A., Cadiou, H., Mason, A., & McNaughton, P. A. (2008). Role of the hyperpolarization-activated current  $I_h$  in somatosensory neurons. *J. Physiol* **586**, 5911–5929.
- Moosmang S, Stieber J, Zong X, Biel M, Hofmann F & Ludwig A (2001). Cellular expression and functional characterization of four hyperpolarization-activated pacemaker channels in cardiac and neuronal tissues. *Eur J Biochem* **268**, 1646–1652.
- Parekh A, Campbell AJ, Djoughri L, Fang X, McMullan S, Berry C, Acosta C & Lawson SN (2010). Immunostaining for the  $\alpha 3$  isoform of the Na<sup>+</sup>/K<sup>+</sup>-ATPase is selective for functionally identified muscle spindle afferents *in vivo*. *J Physiol* **588**, 4131–4143.
- Pena F, Amuzescu B, Neaga E & Flonta ML (2006). Thermodynamic properties of hyperpolarization-activated current ( $I_h$ ) in a subgroup of primary sensory neurons. *Exp Brain Res* **173**, 282–290.
- Rodrigues AR & Oertel D (2006). Hyperpolarization-activated currents regulate excitability in stellate cells of the mammalian ventral cochlear nucleus. *J Neurophysiol* **95**, 76–87.

- Santoro B & Tibbs GR (1999). The HCN gene family: molecular basis of the hyperpolarization-activated pacemaker channels. *Ann NY Acad Sci* **868**, 741–764.
- Santoro, B., Chen, S., Luthi, A., Pavlidis, P., Shumyatsky, G. P., Tibbs, G. R., & Siegelbaum, S. A. (2000). Molecular and functional heterogeneity of hyperpolarization-activated pacemaker channels in the mouse CNS. *J. Neurosci.* **20**, 5264–5275.
- Scroggs RS, Todorovic SM, Anderson EG & Fox AP (1994). Variation in  $I_H$ ,  $I_{IR}$ , and  $I_{LEAK}$  between acutely isolated adult rat dorsal root ganglion neurons of different size. *J Neurophysiol* **71**, 271–279.
- Spain WJ, Schwindt PC & Crill WE (1987). Anomalous rectification in neurons from cat sensorimotor cortex in vitro. *J Neurophysiol* **57**, 1555–1576.
- Stieber, J., Stockl, G., Herrmann, S., Hassfurth, B., & Hofmann, F. (2005). Functional expression of the human HCN3 channel. *J. Biol. Chem.* **280**, 34635–34643.
- Takigawa T, Alzheimer C, Quasthoff S & Grafe P (1998). A special blocker reveals the presence and function of the hyperpolarization-activated cation current  $I_H$  in peripheral mammalian nerve fibres. *Neuroscience* **82**, 631–634.
- Tu H, Deng L, Sun Q, Yao L, Han JS & Wan Y (2004). Hyperpolarization-activated, cyclic nucleotide-gated cation channels: roles in the differential electrophysiological properties of rat primary afferent neurons. *J Neurosci Res* **76**, 713–722.
- Ulens C & Tytgat J (2001). Functional heteromerization of HCN1 and HCN2 pacemaker channels. *J Biol Chem* **276**, 6069–6072.
- Viana F, De LaPeña E & Belmonte C (2002). Specificity of cold thermotransduction is determined by differential ionic channel expression. *Nat Neurosci* **5**, 254–260.
- Villiere V & McLachlan EM (1996). Electrophysiological properties of neurons in intact rat dorsal root ganglia classified by conduction velocity and action potential duration. *J Neurophysiol* **76**, 1924–1941.
- Wang, Z., van den Berg, R. J., & Ypey, D. L. (1997). Hyperpolarization-activated currents in the growth cone and soma of neonatal rat dorsal root ganglion neurons in culture. *J. Neurophysiol.* **78**, 177–186.
- Weng, X., Smith, T., Sathish, J., & Djouhri, L. (2012). Chronic inflammatory pain is associated with increased excitability and hyperpolarization-activated current ( $I_h$ ) in C- but not Adelta-nociceptors. *Pain.* **153**: 900–914.
- Womble MD & Moises HC (1993). Hyperpolarization-activated currents in neurons of the rat basolateral amygdala. *J Neurophysiol* **70**, 2056–2065.
- Yao H, Donnelly DF, Ma C & LaMotte RH (2003). Upregulation of the hyperpolarization-activated cation current after chronic compression of the dorsal root ganglion. *J Neurosci* **23**, 2069–2074.

### Author contributions

All work was carried out at the Department of Physiology and Pharmacology, University of Bristol. Conception and design of experiments: S.N.L., L.G., A.H., S.M. and L.D. Collection, analysis and interpretation of data: L.G., S.M. and S.N.L. Drafting the article or revising it critically for important intellectual content: L.G., S.N.L., C.A., A.H. and L.D.

### Acknowledgements

This work was supported by the Wellcome Trust UK, LG was supported by Overseas Research Scholarship, China Scholarship Council and a postgraduate scholarship from The University of Bristol. Thanks to Dr Yuanlong Song for writing analysis scripts, to Dr Xin Fang for contribution to early experiments and to Professor Tim Biscoe for constructive comments on the manuscript.